Size effects on varistor properties made from zinc oxide nanoparticles by low temperature spark plasma sintering

Lena Saint Macary, Myrtil L. Kahn, Claude Estournès, Pierre Fau, David Trémouilles, Marise Bafleur, Philippe Renaud, Bruno Chaudret

Size effects on varistor properties made from zinc oxide nanoparticles by low temperature spark plasma sintering

By *Léna Saint Macary*, [†§] *Myrtil L. Kahn*,[†]* *Claude Estournès*;[‡] *Pierre Fau*[†], *David Trémouilles*,[¤] *Marise Bafleur*,[¤] *Philippe Renaud*,[§] and *Bruno Chaudret*[†]*

† Dr. B. Chaudret, Dr. M. Kahn, Dr. P. Fau, L. Saint Macary

Laboratoire de Chimie de Coordination, UPR8241 CNRS,

205 route de Narbonne, F-31077 Toulouse, France

E-mail : kahn@lcc-toulouse.fr, chaudret@lcc-toulouse.fr

‡ Dr. C. Estournès

Centre Interuniversitaire de Recherche et d'Ingénierie des Matériaux & Plateforme Nationale de Frittage Flash, Module de Haute Technologie, Université Paul Sabatier,

118 route de Narbonne, F-31062 Toulouse, France

§ Dr. P. Renaud, L. Saint Macary

Freescale Semiconductor,

134 avenue du Général Eisenhower, F-31023 Toulouse, France

¤ Dr. M. Bafleur, Dr. D. Trémouilles

LAAS-CNRS, Université de Toulouse,

7 avenue du Colonel Roche, F-31077 Toulouse, France.

ABSTRACT:

Conditions for the elaboration of nanostructured varistors by Spark Plasma Sintering (SPS) are investigated, using 8 nm zinc oxide nanoparticles synthesized following an organometallic approach. A binary system constituted of zinc oxide and bismuth oxides nanoparticles is used for this purpose. It is synthesized at room temperature in an organic solution through the hydrolysis of dicyclohexylzinc and bismuth acetate precursors. Sintering of this material is performed by SPS at various temperatures and dwell times. The determination of the microstructure and the chemical composition of the as prepared ceramics are based on Scanning Electron Microscopy (SEM) and X-Ray Diffraction (XRD) analysis. The non linear electrical characteristics are evidenced by current-voltage (I-V) measurements. The breakdown voltage of these nanostructured varistors strongly depends on grain sizes. The results show for the first time that, nanostructured varistors are obtained by SPS at sintering temperatures ranging from 550 to 600°C.

Keywords: Organometallic, Zinc oxide, Nanoparticles, Spark plasma sintering, Varistor

1. Introduction

Zinc oxide (ZnO) is characterized by remarkable optical, thermal, electronic and chemical properties. It is a wide band gap (3.37 eV at room temperature) II-VI n-type semiconductor displaying many applications, from solar cell electrodes,[1] which take advantage of both its optical transparency in the visible range and conductivity in thin film form, to the exploitation of high electromechanical coupling constant values as piezoelectric transducers.[2] ZnO remains the subject of many research works. A central issue consists in doping this material; first because p-doping is a prerequisite for its use in optoelectronics and also because obtaining an experimental proof of the calculated ferromagnetism at room temperature of ZnO doped with 3d transition metals is still a challenging issue.[3] Among these present and future applications, ZnO ceramics associated with other additive oxides are well known to work as varistors, *i.e.* these are devices which exhibit non-linear current-voltage (I-V) characteristics.[4, 5] Such micrometric ZnO-based varistors are widely employed and commercialized to protect electrical equipments operating at various voltage levels from degradations caused by overvoltage peaks and electrostatic discharges such as the ones related to lightning events in aeronautics applications.

From a practical point of view, it is usually accepted that the protection voltage is proportional to the number of grain boundaries.[6] The expansion of nanoscience over the last decades stimulated chemists so that a wide variety of nanoobjects were developed and are now available by the so called bottom-up approach.[7] Such structures have attracted much interest in the varistor world for the design of high quality devices since size and microstructure control are key parameters for the elaboration of non linear ceramics.[8] They proved useful to improve electrical characteristics, in particular breakdown field. However such polycrystalline materials usually undergo a growth of their grain size during sintering[9] and the initial nanoscale is lost in the final ceramics so that no varistor ceramics with mean

diameter grain size below 100 nm (nanostructured varistors) have been reported. The finest grained varistor ceramics described in the literature contain grains in the range of 250 to 500 nm in diameter.[10, 11] The aim of the present study is therefore to explore new process allowing the realization of nanostructured varistors.

Here is reported the use of ZnO nanoparticles synthesized by an organometallic method for the design of nanostructured varistors. This method allows a good control over the size and surface state of the particles. In the present work, the most widespread varistor forming oxide, namely bismuth oxide (Bi_2O_3), is the only added constituent for the manufacture of ceramic parts. They are thus expected to exhibit only low non linearity coefficients. Interestingly, the nanometric scale of the grains was preserved by the use of a non conventional sintering technique: Spark Plasma Sintering (SPS).

2. Experimental part

2.1. Synthesis:

Pure zinc oxide materials:

Two equivalents of water were added dropwise to a 4.32 M THF solution of [$ZnCy_2$] *via* a wet solution of THF containing 10300 ppm of water. After the solution turned dark yellow, a white solid precipitates within minutes. THF is evaporated to dryness under vacuum. A white powder is obtained.

Zn/Bi mixed metal oxide materials:

A 0.08 molar equivalent of bismuth triacetate (III) were added to a 4.32 M THF solution of [$ZnCy_2$]. The solution is kept under stirring during 10 minutes in order to achieve the complete dissolution of bismuth triacetate (III). Two equivalents of water were then added dropwise. The solution turns yellow then white and a precipitate forms. The powders were dried under vacuum and then annealed at 400°C for 4h under air.

2.2. XRD:

The powder's and pellet's X-ray diffraction patterns were collected on a XPert Pro (Theta-Theta mode) Panalytical diffractometer with λ(CuKα1, Kα2) = 1.54059, 1.54439 Å, respectively. The extraction of peak positions for indexing was performed with the fitting program, available in the PC software package Highscore+ supplied by Panalytical. The phase identification was performed with 'searchmatch' in Highscore+, based on the PDF2 ICCD database.

2.3. TEM/SEM:

The TEM specimens were prepared by slow evaporation of solution droplets of the different samples deposited on carbon-supported copper grids. The experiments were performed on a JEOL JEM-1011.

The size distribution was determined manually by an analysis of low-magnification TEM images. In this procedure, the different particles were visually identified according to an upper and lower intensity threshold and then counted and measured. This analysis was made only on isolated particles which are not numerous in the case of agglomerated particles, thus giving only an estimate of the particle size.

SEM specimens were prepared as follows: the powder samples were either deposited on a silicon substrate or glued directly on the aluminum sample holder *via* a silver paste. Pellets were directly stuck to the aluminum sample holder by a carbon-double-face tape. SEM measurements were performed on a field emission gun scanning electron microscope JEOL 6700F. Micrographs were collected using secondary electron imaging (SEI) for the topographical mode and in compositional mode by back-scattered electron imaging (BEI). X-

ray analysis was performed using the SEM interfaced with a Princeton Gamma-Tech energy dispersive X-ray (EDX) microanalysis system.

2.4. Sintering:

Classical sintering:

Pellets were prepared by uniaxial pressing ZnO powders in a 5 mm diameter die. Usual sintering process under air was performed in a compact tube furnace RS50/300/11 from Nabertherm equipped with a C40 program controller at a maximum temperature ranging from 850 to 1000°C. The heating rate from room temperature to 400°C is 1°C.min^{-1}; above 400°C the temperature is raised by 2°C.min^{-1} up to the maximum temperature which is held for 2h. The cooling rate is 1.5°C.min^{-1}.

Spark Plasma Sintering:

Samples were sintered using a Dr Sinter 2080 SPS apparatus (SPS Syntex Inc., Tokyo, Japan). Precursor's powders (without any sintering aids) were loaded onto an 8-mm inner diameter cylindrical die and placed in a chamber under vacuum. The pulse sequence was 12-2 (pulses–dead time or zero current), with each pulse lasting 3.3 ms. The temperature was automatically raised from room temperature, monitored and regulated to the final temperature (500-800°C range) by thermocouple introduced in a small hole located at the surface of the die. A heating rate of 50°C.min^{-1} was used to reach the final temperature. The cooling conditions are not forced: once the maximum temperature is reached, heating is stopped and the pellets are left to cool down to room temperature. Uniaxial pressure of 50 MPa was applied progressively in the first minute and held until completion of the temperature step at final temperature (held from 0 to 15 minutes). In these conditions, the current passing through the die and the voltage reached maximum values of applied values of 300 A and 3 V, respectively.

2.5. Electrical measurements:

The sintered pellet surfaces were polished using various grades of SiC abrasive papers (Presi P600 and P1200) down to a thickness of about 1 mm in order to eliminate the carbon surface contamination induced by the use of graphitic dies. Gold electrodes were further deposited on both sides of the pellets by sputtering on an Alcatel 450 sputtering machine. Electrical measurements were performed on a HP4142B Modular DC Source Monitor limited to 200 V in absolute value. These measurements were completed when necessary on a 370A Programmable Curve Tracer from Sony Tektronix attaining 2000 V.

3. Results

3.1 Synthesis:

In order to test the effect of bismuth oxide addition on zinc oxide based ceramics, we first synthesized nanometric zinc oxide powder as a reference sample. This was achieved by decomposition of an organometallic precursor in solution, namely the dicyclohexyl zinc compound, [$ZnCy_2$], in THF. The precursor is hydrolyzed by controlled introduction of water in the solution kept under argon. If only one equivalent of water is added to the reaction medium, a yellow air sensitive precipitate forms which turns white when placed in contact with air or upon addition of another equivalent of water. Two equivalents of water are necessary to complete the direct formation of the final white ZnO product in solution. Once the solvent was removed by evaporation under vacuum, the white solid (Sample 1) was characterized by TEM as agglomerated nanoparticles (see Figure 1a) of approximate diameter 10 nm.

Bismuth oxide is known as one of the so-called varistor forming oxides when associated to zinc oxide in ceramics. The varistor properties arise from the segregation of

bismuth atoms at the interfaces between zinc oxide grains.[12] Consequently, we focused on granting the homogeneous distribution of bismuth at the nanometric scale in the synthesized powders. Thus, we performed the codecomposition of the same organozinc precursor and a bismuth salt, namely bismuth acetate, in a one step controlled hydrolysis. The intermediate yellow product discussed hereabove also forms. The obtained particles (Sample 2) are similar in size and shape with Sample 1 ones, but these two samples differ in terms of agglomeration. Sample 2 is composed of well-defined isotropic nanoparticles (see Figure 1b).

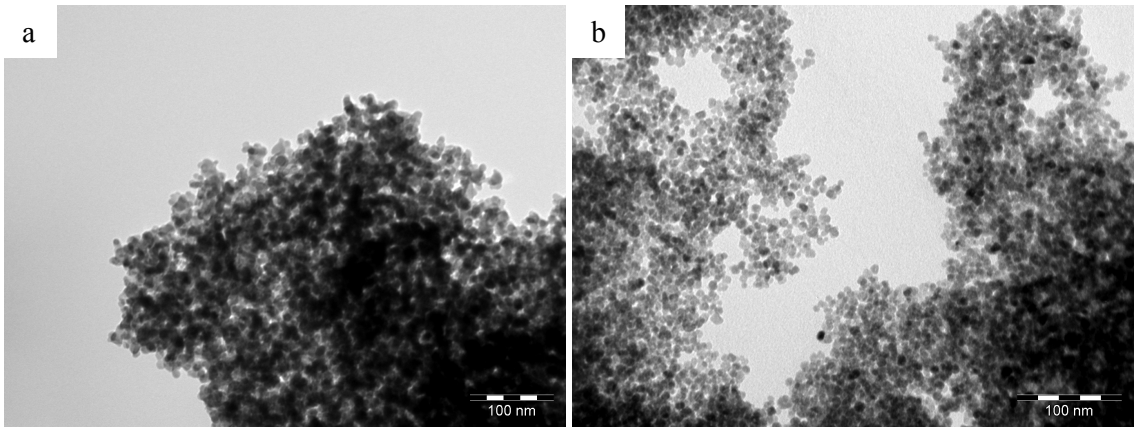

Figure 1: TEM micrographs of nanoparticles syntheses of: a) Sample 1; b) Sample 2

XRD characterization of the as-obtained powders identifies both for Sample 1 and Sample 2, a würtzite zinc oxide phase (see Figure 2a and 2b respectively). The extent of the crystalline domains is larger in Sample 1 than in Sample 2. Sample 2 diffractogram shows an additional peak situated around 30° corresponding to bismuth. However, no clues are given concerning the phase under which bismuth is found since the peak is too broad to be analyzed. In order to gain access to more information concerning this phase, the hydrolysis of bismuth acetate alone in THF was performed and the resulting white powder analyzed by XRD. The diffractogram indicated the presence of bismuth oxoacetate and unreacted bismuth acetate (see supplementary materials, S1). It is however difficult to conclude on the presence or not of bismuth acetate in this case. Indeed, the most intense peak of bismuth oxide in its beta phase

is also situated at similar angle values. High resolution transmission electronic microscopy (HRTEM) was performed on Sample 2 but the bismuth based phase was not located. Once dried, the nanoparticles of Sample 2 were submitted to post-synthesis annealing treatment at 400°C for 4h (Figure 2c). All the diffractograms display characteristic peaks of the hexagonal zincite phase (space group $P6_3mc$) in the 30° to 80° 2θ range. These peaks have narrowed indicating crystallite growth. Additional peaks appeared; and were clearly identified as bismuth oxide in the beta allotropic form (Figure 2c). The width of the corresponding peaks suggests that the β-Bi_2O_3 crystallites are larger than zinc oxide ones.

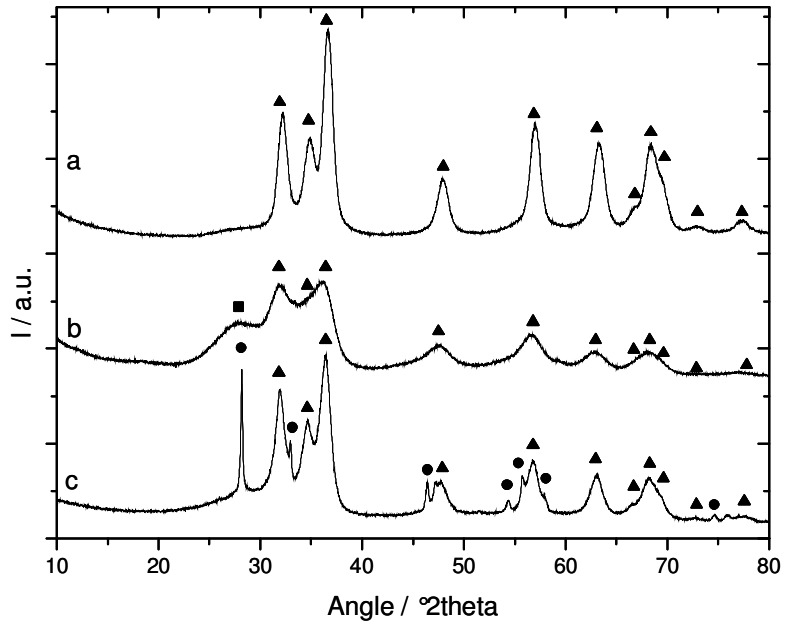

Figure 2: X-Ray diffractograms: a) Sample 1 as prepared; b) Sample 2 as prepared; and c) Sample 2 after annealing at 400°C (▲ ZnO, ● β-Bi_2O_3, ■ not defined)

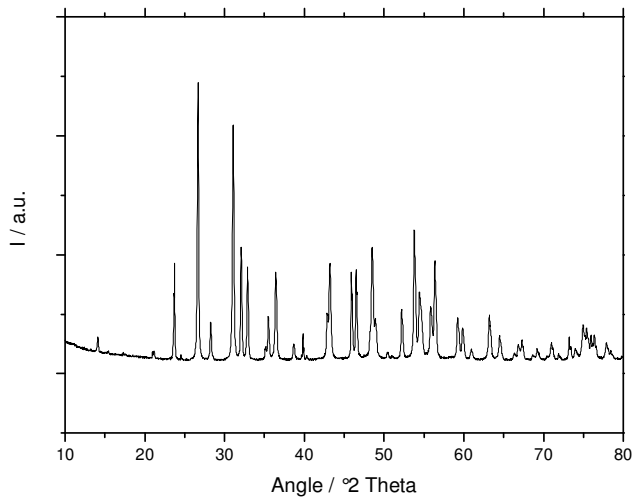

S1: X-Ray diffractogram of the product obtained by direct hydrolysis of bismuth acetate

3.2. Sintering:

The next step consisted in making dense nanoceramics from these nanostructured powders in order to study their electrical characteristics. Attempts to sinter pure ZnO nanopowders (Sample 1), once shaped into pellets by pressing at 3 tons, were first carried out in a furnace at temperatures ranging from 800 to 1000°C for 2h. The as-prepared pellets are highly porous, their densities hardly reach 30% of pure zinc oxide (figure 4a). A second technique, namely spark plasma sintering (SPS), was considered. It consists in hot pressing at very high heating rates. Various final temperatures and holding times were tested both for the reference powder (Sample 1) and bismuth containing powder (Sample 2). The experimental conditions are summarized in Table 1.

Pellet	Sample	Sample annealing	Sintering T_{max}[°C] /Step time [min]	Density [$g.cm^{-3}$]	Density [%]	SEM Grain size [nm]	XRD cristallite size [nm]
1	1	∅	600/0	3.8	67	~10	
2	1	∅	800/0	4.7	82	~100	

3	1	∅	900/0	5.2	91	~2000-5000	
4	2	400°C	500/15	4.1	65	~15	22
5	2	400°C	550/15	5.2	83	~30-50	31
6	2	400°C	600/4	4.6	73	~25	35
7	2	400°C	600/15	6.1	97	~300-500	75
8	2	400°C	650/15	5.9	94	~1000	72
9	2	400°C	800/0	5.7	91	~1000	98
10	2	400°C	800/0	5.8	92	~1000	83
11	2	400°C	900/0	5.6	89	~3000-5000	>100

Table 1 : Data of the pellets prepared by SPS

During SPS, thermal shrinkage is monitored by a dilatometer, which allows to get insights on the sintering process. Sintering profiles considerably differ depending on the powder composition as illustrated in Figure 3. For example, Sample 1 densification occurs between 700 and 750°C (Figure 3a), whereas bismuth containing powder (Sample 2) undergoes significant shrinkage at lower temperatures, between 400 and 650°C (Figure 3b). The important displacement observed at low temperature for Pellet 2 compared to Pellet 11 is mainly due to the fact that initial compaction prior to SPS is carried out manually. The fact that Sample 1 was not annealed prior to sintering may also partly explain this difference as the amount of adsorbed species may be higher in this case.

Final densities of the pellets were measured using the water immersion method. Pellets made from Sample 1 are all the more dense as the applied temperature is high. A densification of 90% of the theoretical density of zinc oxide (5.7 $g.cm^{-3}$) was reached at the maximum temperature of 900°C applied for this study. For Sample 2, it can be noted that the theoretical density (6.4 $g.cm^{-3}$) is higher than that of pure zinc oxide due to the amount of bismuth oxide. The trend concerning the variation of density with temperatures for this composition (Sample 2) is different from that followed by pure zinc oxide materials (Sample 1) for which density

increases with the sintering temperature increase. Indeed, for Sample 2, pellets made at 800°C are denser than the ones sintered at 900°C (Table 1). Moreover, a step at final temperature for several minutes was found to have a considerable impact on sintering, yielding very high densities at temperatures as low as 600°C.

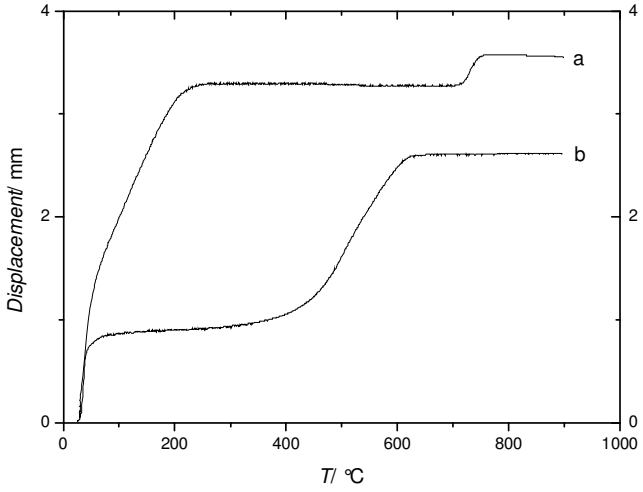

Figure 3: Sintering profiles of: a) Pellet 2 made from Sample 1; b) Pellet 11 made from Sample 2

The pellets' microstructure was observed by SEM. Figure 4(a-g) shows characteristic SEM images of ceramics sintered from Sample 1 and Sample 2 at various temperatures. Pellets prepared from Sample 1 by SPS at 800°C considerably differ from those sintered in a classical furnace at 1000°C in terms of density (4.7 and 1.7 $g.cm^{-3}$ respectively), their grain sizes, however are similar and about a few hundred nanometers as shown in Figure 4a and 4b.

Grain size increase with temperature is observed for each powder composition. For example, Pellet 1 grains, corresponding to the sintering of Sample 1 at 600°C (Figure 4b), are in the range of a few tens of nanometers whereas Pellet 2 and Pellet 3, which were also made from Sample 1, exhibit grains of about 100 nm and 1 µm respectively as a result of SPS treatment at 800°C for Pellet 2 and 900°C for Pellet 3. The same trend is observed for bismuth

containing samples. In the case of Sample 2, SPS sintering at 600°C (Pellet 6) and at 800°C (Pellet 10) yields grains of about 50 nm (Figure 4f) and 1 μm (Figure 4g) respectively. Grain size and density are also considerably modified with dwell time, as illustrated at 600°C by the difference between Pellet 6 and Pellet 7 maintained at the final temperature for 4 and 15 minutes, respectively. A grain size increase of an order of magnitude occurs and is associated with an increase in density in Pellet 7, globally resulting from a decrease in porosity (see Table 2). In micrometric ceramics, bismuth-rich phases are generally found to be located at multiple grain boundaries.[13, 14] Backscattered Electron Imaging (BEI) micrographs (Figure 4g) provide a view of the repartition of the elements in the pellets by chemical contrast imaging. Bismuth-rich phases appear in white and zinc oxide in gray, which is evidenced by X-ray microanalysis (see supplementary material, S2). This method shows that in pellets sintered by SPS at high temperature, thus undergoing grain growth up to the micrometric size, bismuth is mainly found to stand at the multiple grain junctions (Figure 4h). Some grain junctions exhibit larger amounts of bismuth, but the distribution of bismuth inside the material appears homogeneous. For Pellet 5 and Pellet 6, BEI can not be performed at these magnifications however two phases can be distinguished. It can be assumed that polyhedral well faceted grains correspond to zinc oxide, the second interpenetrated phase being identified as bismuth rich phase.

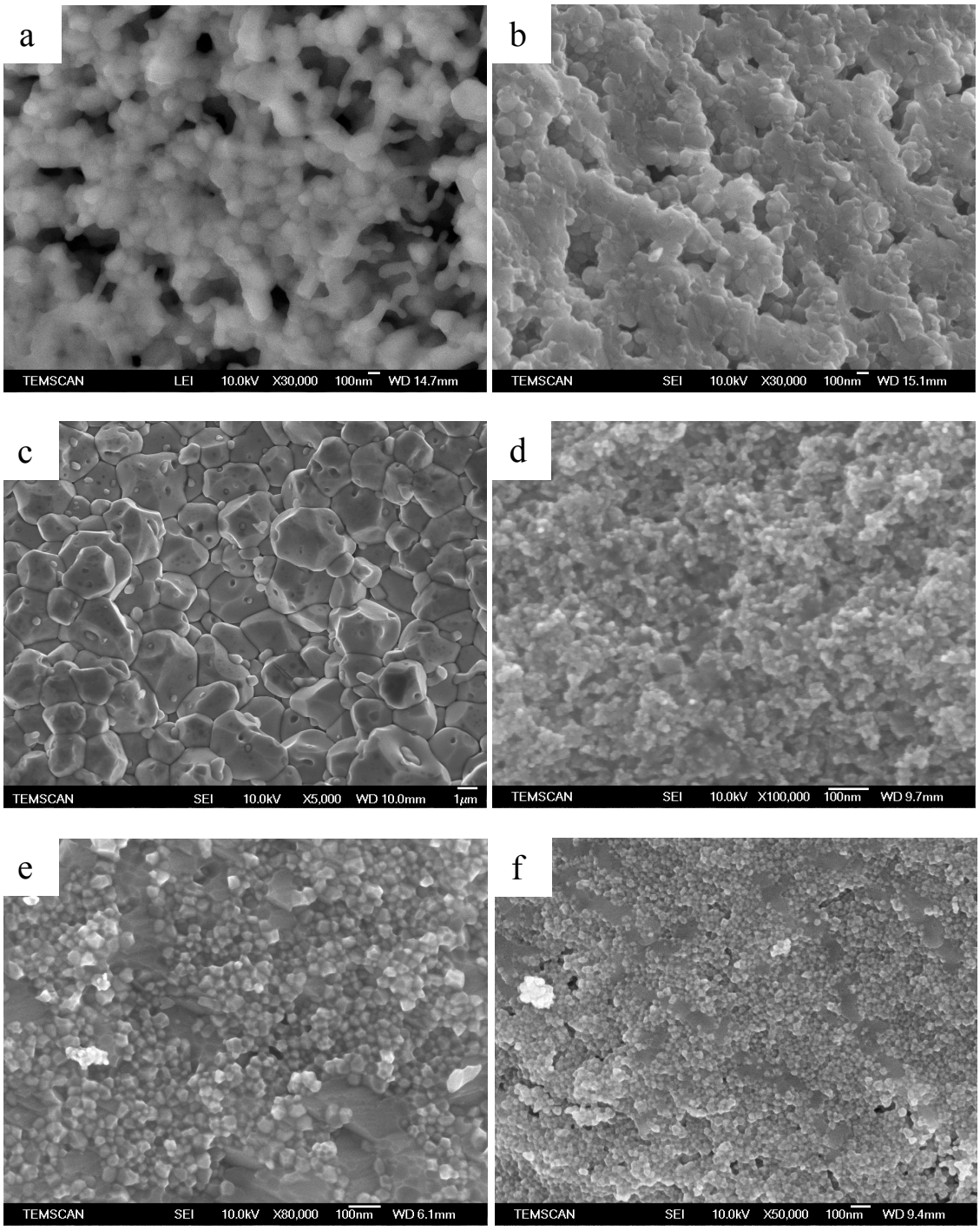
a
TEMSCAN LEI 10.0kV X30,000 100nm WD 14.7mm
b
TEMSCAN SEI 10.0kV X30,000 100nm WD 15.1mm
c
TEMSCAN SEI 10.0kV X5,000 WD 10.0mm 1μm
d
TEMSCAN SEI 10.0kV X100,000 100nm WD 9.7mm
e
TEMSCAN SEI 10.0kV X80,000 100nm WD 6.1mm
f
TEMSCAN SEI 10.0kV X50,000 100nm WD 9.4mm

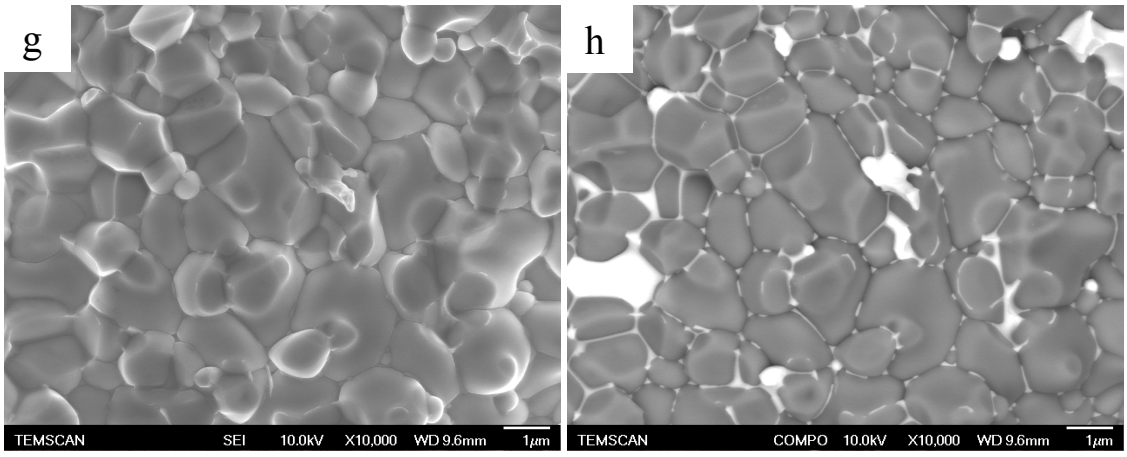

Figure 4: SEM SEI micrographs of fracture surface of: a) Sample 1 sintered at 1000°C in a furnace; b) Pellet 2, Sample 1 sintered by SPS at 800°C; c) Pellet 3, Sample 1 sintered by SPS at 900°C; d) Pellet 1, Sample 1 sintered by SPS at 600°C; e) Pellet 5, Sample 2 sintered by SPS at 550°C for 15 minutes; f) Pellet 6, Sample 2 sintered by SPS at 600°C for 4 minutes; g) Pellet 10, Sample 2 sintered by SPS at 800°C; h) SEM BEI micrograph of the same image as (g)

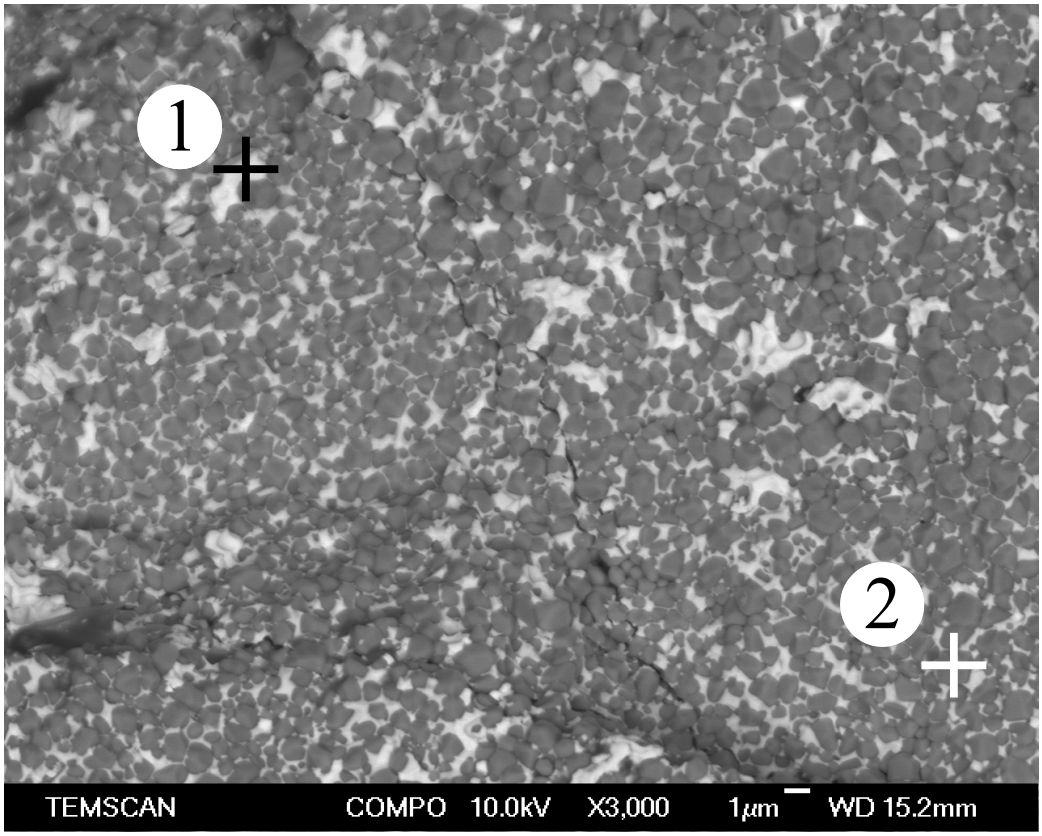

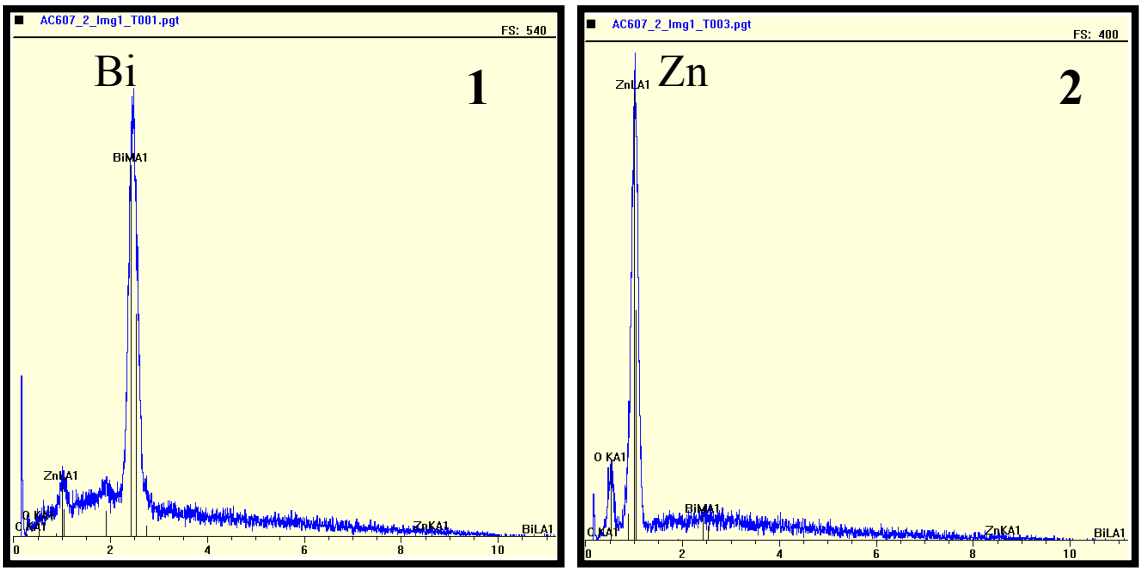

S2: EDX analysis on a backscattered image of: 1) a white zone and 2) a dark zone

Figure 5 shows the XRD diagrams of pellets sintered by SPS at various temperatures. All diffractograms display the characteristic pattern of zincite phase in the 30° to 60° 2θ range. Additional peaks result from the presence of bismuth containing phases or surface carbon contaminants (at 26.5 and 54.5°), this contamination comes from the SPS die and is further eliminated by polishing. When Pellet 4 is formed by sintering at 500°C for 15 minutes, a phase transformation of bismuth oxide occurs from beta in the pristine annealed powder to alpha phase in the pellet (Figure 5a). At higher temperature, namely 600°C, bismuth oxide has further transformed into γ-Bi_2O_3 or $Bi_{38}ZnO_{58}$ ($19Bi_2O_3$:ZnO) and two other new species which are identified as metallic bismuth : one is rhombohedral (R-3m) and the other is cubic (Pm-3m). The phases γ-Bi_2O_3 and $Bi_{38}ZnO_{58}$ have identical crystal structures and can be only distinguished by a slight shift in the XRD patterns.[15] Consequently, the small intensity and large width of the corresponding peaks do not allow to discriminate between these two bismuth oxide phases. At the intermediate temperature of 550°C, a mixture of α-Bi_2O_3, γ-Bi_2O_3 or $Bi_{38}ZnO_{58}$ and cubic bismuth is found (not shown). As for pellets sintered at 800°C

and above, bismuth is exclusively present in the rhombohedral metallic phase. The diffraction peak half-height widths of zinc oxide narrow with sintering temperature as a consequence of crystallite growth. The crystallite size was estimated using the Debye-Scherrer equation up to 100 nm since above this value the equation is no more valid due to the internal line width of the diffractometer. These calculations are in good agreement with SEM grain size observations for finely grained pellets such as Pellet 4, Pellet 5 and Pellet 6. For instance, Pellet 5 was found to contain 30 nm large crystallites which is the grain size seen on SEM images (Figure 4e). For pellets made at higher temperatures the crystallite size calculated and grain size observed do not match; the grain size being larger than the calculated value. This suggests that the micrometric grains observed by SEM are polycristalline. In order to obtain a varistor, we annealed the pellets under air so as to turn the metallic bismuth phase into an oxide phase. This treatment is performed at 650°C for 10h and the temperature is raised at 1°C.min^{-1}. After annealing of these pellets under air at 650°C for 10h (see Figure 4d), metallic bismuth turned into γ-Bi_2O_3 or $Bi_{38}ZnO_{58}$. The main bismuth-rich phase usually found in varistor ceramics made by classical sintering is the β–Bi_2O_3 phase,[10, 16] but the presence of δ, γ and α phases are also reported in some studies depending on the additives and thermal processing conditions.[17-20] At a temperature of 650°C, bismuth oxide and zinc oxide do not form the eutectic so that no additional sintering and no grain growth occur.

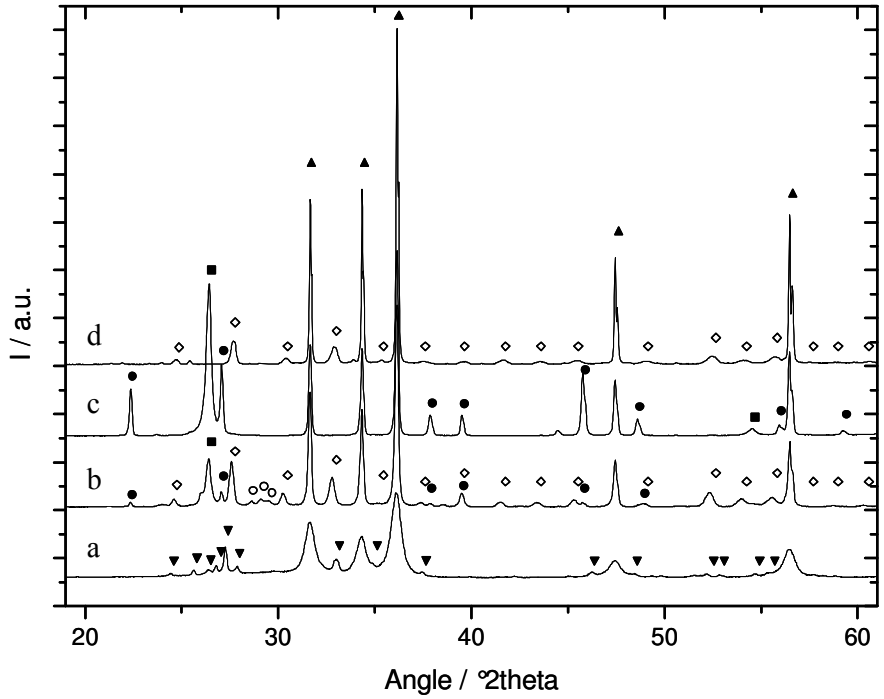

Figure 5: XRD diffractograms for: a) Pellet 4 sintered at 500°C b) Pellet 7 sintered by SPS at 600°C; c) Pellet 9 as sintered at 800°C; and d) Pellet 9 after annealing at 650°C (▲ ZnO, ■ C, ▼ α-Bi_2O_3, ◊ γ-Bi_2O_3 or $Bi_{38}ZnO_{58}$, ● Bi, ○ Bi)

To sum up the results, ceramics are formed by SPS from binary bismuth oxide and zinc oxide nanostructured powders. After annealing of these powders, sintering is performed by SPS at low temperature as shrinkage occurs between 400°C and 650°C. By this method, nanometric grain sized ceramics are obtained between 500 and 600°C. Simultaneously with densification of the pellets, bismuth oxide undergoes phase transformation into metallic bismuth. The metallic bismuth phase is turned into the oxide phase again by post sintering annealing.

3.3. Electrical characteristics:

Polycristalline ceramics (Pellet 1, Pellet 2 and Pellet 3) prepared from pure ZnO powder (Sample 1), exhibit linear I/V characteristics with resistivities of about 20 Ω.cm. This value is slightly higher than that of pure monocristalline zinc oxide, which generally ranges from 1 to 10 Ω.cm.[21] Pellets prepared from bismuth containing powders (Sample 2) do not always show non-linear behavior. Indeed, a resistive behavior is observed for pellets that have not subsequently been annealed under air after sintering. For instance, Pellet 9 and Pellet 10 prepared under the same conditions have radically different electrical behavior as Pellet 10 was not annealed after sintering.

For pellets exhibiting non linear characteristics, following a widespread convention we determine the breakdown field as the field at which a current density of 1 $mA.cm^{-2}$ is measured. The non linearity coefficient α is defined as the slope of the logJ = f(logE) curve between 1 and 10 $mA.cm^{-2}$. When the upper value of current density could not be reached, α was taken as the slope between 1 $mA.cm^{-2}$ and the last recorded point.

The results of the annealed pellets are reported in Table 2. Some annealed pellets show linear electrical behavior, namely Pellet 4 and Pellet 11. Their resistivities are also given in Table 2.

Pellet	T_{max} [°C] / step time [min]	Grain size [nm]	Cristallite size [nm]	α	V_b [$V.cm^{-1}$]	ρ [kΩ.cm]
4	500/15	~15	22	N.A. (non applicable)	N.A.	550
5	550/15	~50	31	NM (non measureable)	>19000	N.A.
7	600/15	~300-500	75	5.8	10660	N.A.
8	650/15	~1000	72	5.6	10955	N.A.
9	800/0	~1000	98	3.6	1565	N.A.
11	900/0	~3000-5000	>100	N.A.	N.A.	2

Table 2: Non linear coefficient (α) and breakdown field (V_b) or resistivity of the bismuth containing ZnO ceramics, annealed after SPS

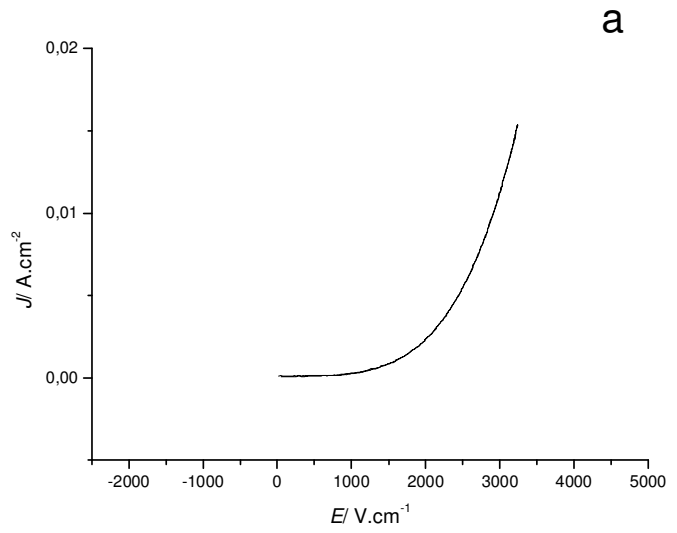

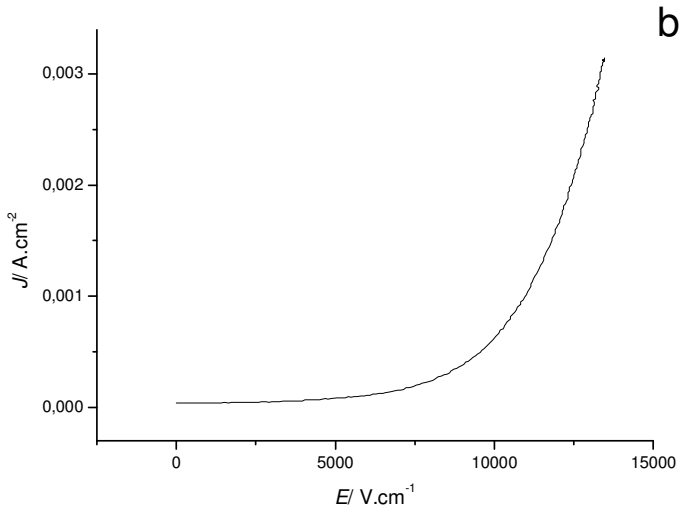

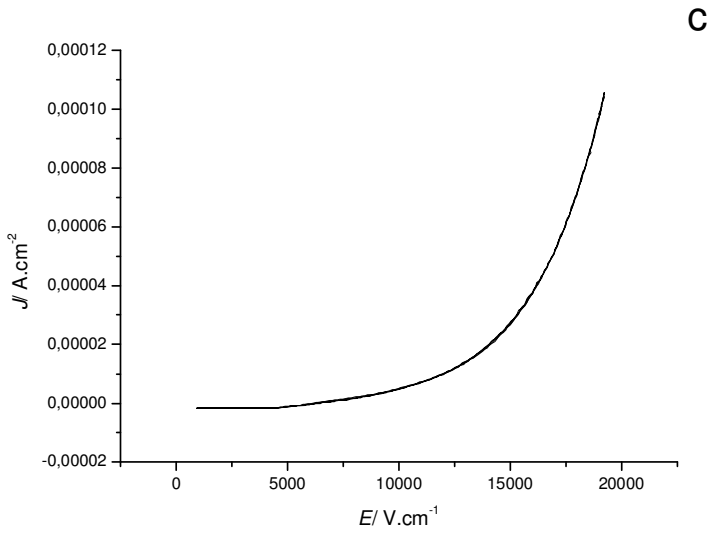

Figure 6: I/V curves of: a) Pellet 9; b) Pellet 8 and c) Pellet 5

Depending on the SPS parameters, pellets annealed after sintering show different electrical behavior. Pellet 4 and Pellet 11 sintered at 500 and 900°C respectively exhibit a linear behavior (see supplementary materials, S3) whereas all ceramics sintered at intermediate temperatures display a non linear varistor behavior (Figure 6). For pellets exhibiting a non linear behavior, overall alpha values are low as a consequence of the simple binary composition and range from 3.6 to 5.8. The characteristic breakdown field depends on grain size observed by SEM, as generally reported. However, there is a discrepancy between Pellet 8 which has micrometric grain size and a V_b exceeding 10000 $V.cm^{-1}$ and Pellet 9 which has similar grain sizes but shows a ten times lower breakdown field. This point will be further discussed. Measurement setup limitation did not allow to extract full electrical characteristics of Pellet 5. For this pellet, the current density hardly reaches 0.1 $mA.cm^{-2}$ at the maximum measurable electric field of 19000 $V.cm^{-1}$. Therefore, breakdown field and non linearity coefficient could not be determined using the conventional criteria. A non linear

behavior is however observed and though current density attained is not sufficient, it can be asserted that breakdown field is far above 19000 $V.cm^{-1}$.

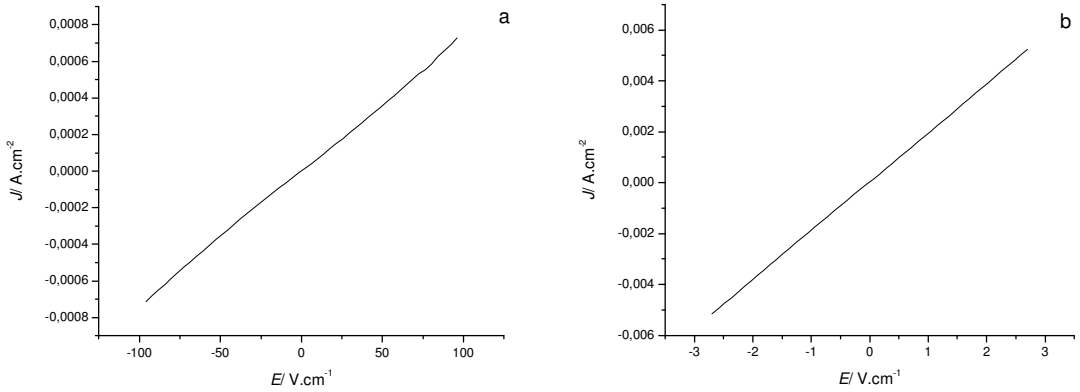

S3: Electrical characteristics of: a) Pellet 4; b) Pellet 11

4. Discussion

4.1 Synthesis

The synthesis of nanoparticles reported here is an adaptation of the method we previously described.[22, 23] This reaction involves the hydrolysis of the organometallic precursor [$ZnCy_2$] in solution. The main improvement consisted in performing a controlled hydrolysis reaction by adding dropwise an organic solution containing two equivalents of water under inert atmosphere so as to grant the reproducibility of hydrolysis conditions. Moreover, to meet the goals of this work, namely the preparation of nanostructured varistors from wet organometallic chemistry, the synthesis has been developed so as to fulfill the requirements of the SPS technique. First of all, in order to provide sufficient amounts of material (grams) for sintering while using reasonable quantities of solvent for the synthesis, the concentration of the reacting solution is multiplied by more than ten. Finally, we gave up the use of stabilizing agents such as amine ligands, because they cause the powders to leak out of the SPS die at low temperature. When [$ZnCy_2$] alone is hydrolyzed without surfactants (Sample 1), the only

possible stabilizing agent is the solvent itself which turns out to be efficient enough to yield nanoparticles but not to keep them in colloidal state as they agglomerate and precipitate. The case of Sample 2 which involves the co-hydrolysis of dicyclohexylzinc and bismuth acetate is, however, somehow different because of the presence of acetate in the reaction solution. The hydrolysis of the bismuth salt releases acetic acid that may account for the less agglomerated state of the nanoparticles. Indeed, carboxylic acids are likely to stabilize nanoparticles synthesized by this organometallic method, since long chain alkyl carboxylic acids acids are widely employed.[24, 25]

We chose to start our study with the most studied oxides used in the formulation of varistors, namely zinc and bismuth oxides. Regardless of non linearity coefficient, we essentially focused on making nanostructured varistors and studying the influence of the enhanced number of grain boundaries per thickness unit on breakdown field. Usually, the amount of bismuth oxide used for varistor ranges from 0.5 to 1 mol %.[14, 16, 26] The surface by volume ratio is considerably higher in the case of nanoparticles when compared to micrometric powders. Therefore, we adapted the bismuth precursor quantity accordingly and focused our study on 0.08 molar equivalents of bismuth precursor for the synthesis of the particles which corresponds to 3.7 mol % Bi_2O_3.

4.2 Nanoparticles for varistor elaboration and SPS for nanostructured ceramics formation

Several papers report on the use of nanoparticles as building blocks for the formation of high voltage breakdown varistors but the description of nanostructured varistors by classical sintering is lacking. In general, particles ranging from 20 to 50 nm are reported as row materials. These latter however undergo grain growth during sintering to attain 250 nm to *c.a.*

10 µm in the final varistor material.[27, 28] To the best of our knowledge, only one paper reports the preparation of a varistor starting from zinc oxide nanoparticles as small as 8 nm.[8] However, in this paper, varistors are sintered by classical method, and due to their high surface reactivity, the nanoparticles grow during sintering and the size of the final grains is very large and equals *c.a.* 10 µm.

We envisioned that by combining the fine organometallic synthesis of few nanometer zinc oxide particles and the fast heating rates of the SPS technique, we might succeed in preparing nanostructured varistors. Indeed, it is well known that SPS allows the formation of well densified ceramics without an excessive grain growth of the starting nanomaterial and limits interdiffusions in the case of materials association.[29-32] For example, nanoceramics of various metal oxide materials such as Al_2O_3,[33] MgO,[34] TiO_2,[35, 36] $BaTiO_3$,[36] ZrO_2,[37] SiAlON,[38] Hydroxy-apatites,[39] Y_2O_3[40] and ZnO[41] have been successfully prepared by this method. In the case of zinc oxide, no nanostructured varistor ceramic has been described mainly because the reported works are either focused on other applications,[41] or the final material is no more nanometric.[42] However Gao et al. report the formation of a nanostructured (~100 nm) ceramic by SPS exclusively made of zinc oxide which exhibits non linear electrical characteristics.[43] We did not observe the same behavior with pure zinc oxide grains: in our case, bismuth oxide introduction was found to be necessary in order to obtain the non-linearity behavior. In the present work, varying SPS temperature and dwell time parameters, we find that in order to keep nanometric-sized grains (i.e. <100 nm) in the presence of bismuth oxide a temperature window between 500 and 600°C is suited. Moreover, density measurements show that among these ceramics, those sintered with a temperature step of 15 minutes were better densified. For example, Pellet 6 sintered at 600°C for 4 minutes is 73% dense whereas Pellet 7, sintered for 15 minutes is 97% dense. A moderate grain growth is associated to this increase in density. Indeed, a final grain size of a few hundred nanometers is

observed for Pellet 7. Our goal being to keep a nanometric grain size as well as to reach the highest possible density of the ceramic, a good balance is found for Pellet 5 which is sintered at 550°C for 15 minutes. In this case, the grain size ranges between 30 and 50 nm and 83% density is reached. This latter value of density is not very high for varistor ceramics, however Pellet 5 showed interesting electrical characteristics (see below).

4.3 Influence of phase transformation on the sintering process SPS

The systematic study of the XRD diagram of the pellets sintered at various temperatures allows establishing that a partial to complete reduction of bismuth oxide into metallic bismuth occurs above 550°C. This unexpected result originates from the particular experimental conditions in which the SPS is performed, *i.e.* the oxide nanoparticles are in a graphitic die that, combined with the low oxygen partial pressure in the chamber under vacuum, can promote the reduction of bismuth oxide. Sintering or annealing a varistor in a reducing atmosphere is known to damage its properties as a result of the collapse of potential barriers at grain boundaries.[44, 45] We also observed such effect, which may even be enhanced in our case by the formation of metallic bismuth creating short circuits, for instance Pellet 10 has a linear electrical characteristic (250 Ω.cm). We overcome this difficulty by annealing the pellets under air after SPS (650°C, 10h) so that for example, Pellet 9, sintered in the same conditions as Pellet 10 but subsequently annealed shows a non linear behavior. Interestingly, this reduction of bismuth oxide into metallic bismuth brings an unexpected sintering aid as it drastically contributes to the densification. For example over 25% of density is gained between Pellet 4 sintered at 500°C, temperature at which the reduction has not begun, and Pellet 5 sintered at 550°C, temperature at which reduced bismuth can be found. The effect of metallic bismuth is also dramatic on the ceramic's morphology. Indeed, pellets sintered

without bismuth, as Pellet 2, exhibit ten times smaller grain sizes than those sintered in the same conditions in the presence of bismuth (see Pellet 9 and Pellet 10 for example). Such results may come from a similar liquid-phase-assisted sintering mechanism that is usually observed at higher temperature when classical sintering is used.[46, 47] Indeed, both XRD and BEI observations confirm the presence of the metallic bismuth phase wetting the ZnO grains (figure 4h). The difference between classical varistor sintering and SPS is that for SPS, the reduction of bismuth oxide into metallic bismuth is likely to form a liquid phase far below the ZnO-Bi_2O_3 binary-system eutectic (740°C). This low temperature formation of a liquid phase accounts for : i) the important densifications obtained at such low temperatures (97% at 600°C in Pellet 7), more than 300°C inferior to the temperature usually reported in the case of classical sintering, ii) the observation of non linearity for I-V characteristics for pellets sintered as low as 550°C.

4.4 Influence of grain size and temperature processing on the electrical characteristics

The electrical characteristics of the annealed pellets exhibit a current density passing through the pellets sintered between 550 to 800°C that does not vary linearly with the applied electric field. The alpha values are comparable with the ones commonly reported in the literature for binary composition restrained to zinc oxide and bismuth oxide (inferior to 8).[48, 49] The breakdown field values (*c.a.* 10000 $V.cm^{-1}$) measured for Pellet 7 and Pellet 8 sintered by SPS respectively at 600°C and 650°C and for which the grain size is evaluated to be equal to 300-500 nm and to 1µm respectively are comparable to the ones reported in the literature for comparable grain size ceramics. Indeed, ZnO varistors containing grains of 250-500 nm, which are the smallest reported in the literature, possess breakdown field values in the range of 15000 to 40000 $V.cm^{-1}$.[11] They were obtained by sintering at 750°C a 2-4 µm thick film.

Similar electrical results are described by Duràn et al. with pellets densified by a two step sintering process at 900°C and 825°C and whose grain size is around 500 nm.[10] In this case, the breakdown field value is in the range of 10000 to 20000 $V.cm^{-1}$.

As expected, we also observed that the breakdown field value greatly depends on the pellet's microstructure, and varies inversely with the average grain size of the ZnO matrix. For example, the breakdown field values increase between Pellet 7 and Pellet 5, and at the same time, the grain sizes decrease by a factor of ten. In the case of Pellet 7 and Pellet 8, the link between the breakdown field value and the grain size is not obvious as they both have the same value of breakdown field although the corresponding grain sizes differ by a factor 2. However, it is well known that the evaluation of grain size from SEM images can only give a rough estimate so that the grain sizes in Pellet 7 and Pellet 8 may actually not greatly differ. Only Pellet 9 does not follow this trend, as it shows low breakdown field value (1500 $V.cm^{-1}$) compared to that of Pellet 8 (11000 $V.cm^{-1}$) whereas both pellets contain grains of the same size. The temperature at which Pellet 9 is formed by SPS (800°C) may be high enough to lead to the evaporation of liquid metallic bismuth similarly to bismuth oxide evaporation occurring in classical sintering.[50] Consequently, the amount of bismuth left is not sufficient to create active potential barriers at all grain boundaries which accounts for the decrease in breakdown field values. Bismuth evaporation also accounts for the linear behavior of Pellet 11 sintered at even higher temperature (900°C). This hypothesis is strengthened by the decrease of the density values measured for Pellet 9 (5.7 $g.cm^{-3}$), sintered at 800°C, and Pellet 11 (5.6 $g.cm^{-3}$), sintered at 900°C, which tend towards the density of pure zinc oxide. The vacuum pressure variations with temperature (see supplementary materials, S4) also endorse the proposal that metallic bismuth evaporates at temperatures above 650°C. Indeed, three pressure increases measured in the vacuum chamber can be distinguished: i) the first one is around 150°C; it is linked to desorption of adsorbed species from the surface of the particles such as water, for

example; ii) the second one occurs between 450°C and 650°C, that is to say in the temperature range at which shrinkage and phase transformations occur. Thus, it may be related to the release of oxygen caused by the reduction of bismuth oxide into metallic bismuth; iii) the last one is recorded between 650°C and 900°C, which we attribute to the evaporation of metallic bismuth.

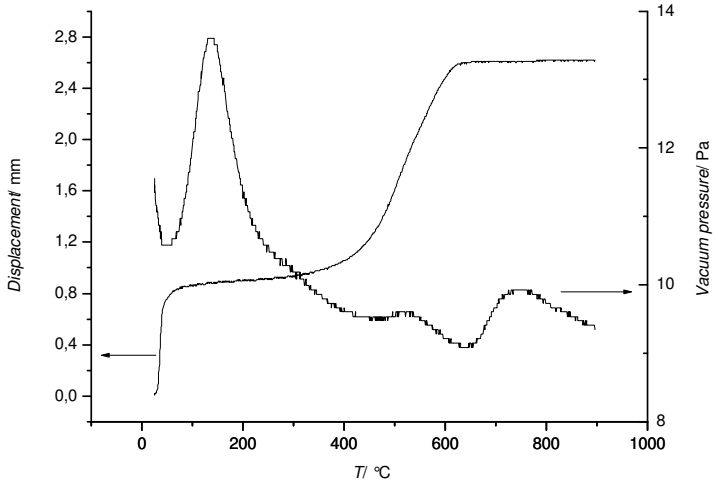

S4: Vacuum pressure variations with temperature and sintering profile simultaneously recorded (Pellet 11)

To the best of our knowledge, no varistor ceramic constituted of grains of size as small as 50 nm was ever elaborated. Pellet 5 sintered by SPS at 550°C is the first example at such low scale. From the non linearity of the curve and the 0.1 $mA.cm^{-2}$ reached at the maximum applicable field (19000 $V.cm^{-1}$), we can assert that the breakdown field value is among the highest ever measured. The number of grains contained in Pellet 5 is 20 times higher than the one contained in Pellet 8 for the same thickness (1 mm). In order to measure the contribution of the same average number of grains in the two above mentioned pellets, Pellet 5 would have to be thinned down to 50 µm, allowing access to an estimated maximum electric field of 300000 $V.cm^{-1}$.

5. Conclusion

Organometallic synthesis provided a ZnO-Bi_2O_3 nanomaterial (10 nm) well suited as a raw material for the formation of two-component varistors. The use of Spark Plasma Sintering (SPS) to shape and densify the powders into pellets results in a reduction of bismuth oxide into metallic bismuth. This constitutes an unexpected and significant sintering aid and promotes low-temperature sintering thus allowing the preparation of nanostructured varistors. These varistors exhibit a non-linear behavior and the dependence of the breakdown field on the material grain size is further demonstrated with a clear shift of the breakdown field to high values observed for nanostructured ceramics. Such an approach has a high potential of development since the versatility of the synthetic approach allows the addition of other oxides known to improve varistor non-linearity (Co, Mn, …).[51-54] This work may open new ways for the elaboration of nanodevices.

Acknowledgement. This research was carried out within the framework of LISPA joint lab between Freescale Semiconductor and the Centre National de la Recherche Scientifique, CNRS supported by the French Ministry of Industry, Midi-Pyrénées Regional Council, Haute-Garonne Council and Grand Toulouse. The authors thank TEMSCAN service for TEM measurements, Vincent Collière for SEM and HRTEM measurements, Ludovic Salvagnac for sputtering deposition and Laure Vendier for XRD measurements.

[1] W. Beyer, J. Huepkes, H. Stiebig, *Thin Solid Films* **2007**, *516*, 147.

[2] Z. L. Wang, *Appl. Phys. A* **2007**, *88*, 7.

[3] C. Liu, F. Yun, H. Morko, *J. Mater. Sci. - Mater. Electron.* **2005**, *16*, 555.

[4] D. R. Clarke, *J. Am. Ceram. Soc.* **1999**, *82*, 485.

[5] T. K. Gupta, *J. Am. Ceram. Soc.* **1990**, *73*, 1817.

[6] M. Bartkowiak, G. D. Mahan, F. A. Modine, M. A. Alim, R. Lauf, A. McMillan, *J. Appl. Phys.* **1996**, *80*, 6516.

[7] Y. Liu, Y. Tong, *Journal of Nanoscience and Nanotechnology* **2008**, *8*, 1101.

[8] M. Singhal, V. Chhabra, P. Kang, D. O. Shah, *Mater. Res. Bull.* **1997**, *32*, 239.

[9] S. C. Pillai, J. M. Kelly, D. E. McCormack, P. O'Brien, R. Ramesh, *J. Mater. Chem.* **2003**, *13*, 2586.

[10] P. Duran, F. Capel, J. Tartaj, C. Moure, *Adv. Mater.* **2002**, *14*, 137.

[11] Y. Q. Huang, L. Meidong, Z. Yike, L. Churong, X. Donglin, L. Shaobo, *Mater. Sci. Eng., B* **2001**, *B86*, 232.

[12] F. Greuter, *Solid State Ionics* **1995**, *75*, 67.

[13] D. R. Clarke, *J. Appl. Phys.* **1978**, *49*, 2407.

[14] K.-I. Kobayashi, O. Wada, M. Kobayashi, Y. Takada, *J. Am. Ceram. Soc.* **1998**, *81*, 2071.

[15] J. P. Guha, Š. Kunej, D. Suvorov, *J. Mater. Sci.* **2004**, *39*, 911.

[16] W. Onreabroy, N. Sirikulrat, A. P. Brown, C. Hammond, S. J. Milne, *Solid State Ionics* **2006**, *177*, 411.

[17] S. Bernik, S. Macek, B. Ai, *J. Eur. Ceram. Soc.* **2001**, *21*, 1875.

[18] S. Ezhilvalavan, T. R. N. Kutty, *Mater. Chem. Phys.* **1997**, *49*, 258.

[19] E. Olsson, G. L. Dunlop, *J. Appl. Phys.* **1989**, *66*, 3666.

[20] E. Olsson, G. L. Dunlop, R. Oesterlund, *J. Appl. Phys.* **1989**, *66*, 5072.

[21] K. Ellmer, *J. Phys. D: Appl. Phys.* **2001**, *34*, 3097.

[22] M. L. Kahn, M. Monge, V. Collière, F. Senocq, A. Maisonnat, B. Chaudret, *Adv. Funct. Mater.* **2005**, *15*, 458.

[23] Miguel Monge, Myrtil L. Kahn, André Maisonnat, B. Chaudret, *Angew. Chem. Int. Ed.* **2003**, *42*, 5321.

[24] Myrtil L. Kahn, Miguel Monge, Etienne Snoeck, André Maisonnat, B. Chaudret, *Small* **2005**, *1*, 221.

[25] C. Pagès, Université Paul Sabatier (Toulouse), **2007**.

[26] E. Olsson, G. L. Dunlop, *J. Appl. Phys.* **1989**, *66*, 4317.

[27] Y. Kang Xue, D. Wang Tian, Y. Han, D. Tao Min, J. Tu Ming, *Mater. Res. Bull.* **1997**, *32*, 1165.

[28] Y. Lin, Z. Zhang, Z. Tang, F. Yuan, J. Li, *Adv. Mater. Opt. Electron.* **2000**, *9*, 205.

[29] M. N. Zhijian Shen, *The Chemical Record* **2005**, *5*, 173.

[30] R. Chaim, M. Levin, A. Shlayer, C. Estournes, *Advances in Applied Ceramics* **2008**, *107*, 159.

[31] M. M. Catherine Elissalde, Claude Estournès, *J. Am. Ceram. Soc.* **2007**, *90*, 973.

[32] U. C. Chung, C. Elissalde, M. Maglione, C. Estournes, M. Pate, J. P. Ganne, *Appl. Phys. Lett.* **2008**, *92*, 042902/1.

[33] R. S. Mishra, J. A. Schneider, J. F. Shackelford, A. K. Mukherjee, *Nanostruct. Mater.* **1995**, *5*, 525.

[34] R. Chaim, Z. Shen, M. Nygren, *J. Mater. Res.* **2004**, *19*, 2527.

[35] P. Angerer, L. G. Yu, K. A. Khor, G. Krumpel, *Mater. Sci. Eng., A* **2004**, *A381*, 16.

[36] M. T. Buscaglia, V. Buscaglia, M. Viviani, J. Petzelt, M. Savinov, L. Mitoseriu, A. Testino, P. Nanni, C. Harnagea, Z. Zhao, M. Nygren, *Nanotechnology* **2004**, *15*, 1113.

[37] U. Anselmi-Tamburini, J. E. Garay, Z. A. Munir, A. Tacca, F. Maglia, G. Spinolo, *J. Mater. Res.* **2004**, *19*, 3255.

[38] X. Xu, T. Nishimura, N. Hirosaki, R.-J. Xie, Y. Yamamoto, H. Tanaka, *Nanotechnology* **2005**, *16*, 1569.

[39] C. Drouet, F. Bosc, M. Banu, C. Largeot, C. Combes, G. Dechambre, C. Estournès, G. Raimbeaux, C. Rey, *Powder Technol.*, *In Press, Corrected Proof*.

[40] R. Chaim, A. Shlayer, C. Estournes, *J. Eur. Ceram. Soc.*, *In Press, Corrected Proof*.

[41] J. Wang, L. Gao, *J. Am. Ceram. Soc.* **2005**, *88*, 1637.

[42] F. Luo, J. He, Y. Lin, J. Hu, *Key Eng. Mater.* **2008**, *368-372*, 514.

[43] L. Gao, Q. Li, W. Luan, H. Kawaoka, T. Sekino, K. Niihara, *J. Am. Ceram. Soc.* **2002**, *85*, 1016.

[44] A. Glot, E. Di Bartolomeo, A. Gaponov, R. Polini, E. Traversa, *J. Eur. Ceram. Soc.* **2004**, *24*, 1213.

[45] E. Sonder, M. M. Austin, D. L. Kinser, *J. Appl. Phys.* **1983**, *54*, 3566.

[46] J.-H. Choi, N.-M. Hwang, D.-Y. Kim, *J. Am. Ceram. Soc.* **2001**, *84*, 1398.

[47] J.-R. Lee, Y.-M. Chiang, *Solid State Ionics* **1995**, *75*, 79.

[48] W. G. Morris, *J. Am. Ceram. Soc.* **1973**, *56*, 360.

[49] J. Wong, *J. Am. Ceram. Soc.* **1974**, *57*, 357.

[50] M. A. de la Rubia, M. Peiteado, J. F. Fernandez, A. C. Caballero, *J. Eur. Ceram. Soc.* **2004**, *24*, 1209.

[51] S. Ezhilvalavan, T. R. N. Kutty, *J. Mater. Sci. - Mater. Electron.* **1996**, *7*, 137.

[52] J. Han, A. M. R. Senos, P. Q. Mantas, *J. Eur. Ceram. Soc.* **2002**, *22*, 1653.

[53] Y. W. Hong, J. H. Kim, *Ceram. Int.* **2004**, *30*, 1301.

[54] W. Onreabroy, N. Sirikulrat, *Mater. Sci. Eng., B* **2006**, *130*, 108.